



Title	Crystal-facet-dependent hot-electron transfer in plasmonic-Au/semiconductor heterostructures for efficient solar photocatalysis
Author(s)	Liu, Guigao; Wang, Tao; Zhou, Wei; Meng, Xianguang; Zhang, Huabin; Liu, Huimin; Kako, Tetsuya; Ye, Jinhua
Citation	Journal of materials chemistry C, 3(29), 7538-7542 https://doi.org/10.1039/c5tc01406a
Issue Date	2015-08-07
Doc URL	http://hdl.handle.net/2115/62627
Type	article (author version)
Additional Information	There are other files related to this item in HUSCAP. Check the above URL.
File Information	Supporting Information.pdf



[Instructions for use](#)

Supporting Information

Crystal-Facet-Dependent Hot-Electron Transfer in Plasmonic-Au/Semiconductor Heterostructures for Efficient Solar Photocatalysis

*Guigao Liu, Tao Wang, Wei Zhou, Xianguang Meng, Huabin Zhang, Huimin Liu, Tetsuya Kako, and Jinhua Ye**

Experimental section

1. Preparation of BiOCl nanosheets exposed {001} and {010} facets

BiOCl nanosheets with exposed {001} and {010} facets (denoted as BiOCl-001 and BiOCl-010, respectively) were selectively prepared via a reported hydrothermal method.^[1] Typically, 6 mmol of $\text{Bi}(\text{NO}_3)_3 \cdot 5\text{H}_2\text{O}$ and 6 mmol of KCl were added in 90 ml water at room temperature forming a mixture solution. Then 1 M NaOH was used to adjust the pH value of the solution to about 6.0. After stirred for 30 min, the mixture solution was transferred into a 120 ml of Teflon-lined stainless autoclave and heated to 160 °C for 24 h. Finally, the resulting products (BiOCl-010) were collected and washed with ethanol and water thoroughly and dried at 70 °C in air. Keeping other conditions identical, the BiOCl-001 was prepared in the absence of NaOH.

2. Preparation of BiOCl-001-Au and BiOCl-010-Au plasmonic photocatalysts

The plasmonic BiOCl-001-Au and BiOCl-010-Au composite photocatalysts were prepared by conventional deposition-precipitation method.^[2] In a typical procedure, 0.5 g of BiOCl nanosheets were added to an aqueous solution of HAuCl_4 (100 ml water containing 0.02 g of $\text{HAuCl}_4 \cdot 4\text{H}_2\text{O}$) neutralized by 0.2 M NaOH. After vigorously stirred for 12 h, the catalysts were separated and exhaustively washed with distilled water, then dried and calcined at 200 °C for 4 h.

3. Sample characterization

The morphology of products was determined by using a JEOL 6701F Field-emission scanning electron microscopy (FESEM) and Tecnai G2 F30 high-resolution transmission electron microscopy (HR-TEM). X-ray diffraction (XRD) was conducted on an X'Pert PRO diffractometer with Cu-K α radiation (PANalytical). The diffuse reflectance spectra of the samples were recorded on a UV-visible spectrophotometer (UV-2600; Shimadzu Corp., Japan) with barium sulfate as the reference. Then the absorption spectra were obtained from the reflectance spectra by means of Kubelka-Munk transformations. N_2 adsorption-desorption experiments were carried out at 77 K to examine the Brunauer-Emmett-Teller surface area (BELsorp II mini, BEL Japan Inc.). Before measuring, the samples were degassed in a vacuum at 150 °C for 12 h. Surface chemical analysis was performed by X-ray photoelectron spectroscopy (XPS, PHI Quantera SXM, ULVAC-PHI Inc., Japan).

4. Photocatalytic aerobic oxidation of 2-propanol

0.1 g of sample was evenly spread over a dish with an area of 5.3 cm² in a 500 mL of a borosilicate glass vessel. Then the interior CO_2 -containing natural air of the vessel was exchanged by artificial air [V(N_2):V(O_2)=4:1]. After the sample was sealed in the vessel, gaseous 2-propanol (iso-propanol, IPA) was injected into the vessel. Prior to light irradiation, the sample was kept in the dark to ensure an adsorption-desorption equilibrium of IPA on the sample. A 300 W Xe arc lamp (10 A imported current, focused through a 45 mm×45 mm shutter window) equipped with a set of glass filters (L42+HA30, 400< λ <800 nm, HOYA Co., Japan) and a water filter was used as the visible-light source for photocatalytic reaction. The concentration of IPA, acetone and CO_2 were analyzed by using an online gas chromatography (GC-2014, Shimadzu Corp., Japan) equipped with FID detectors and methanizer. The apparent quantum efficiencies (AQE) were measured at various monochromatic lights which were obtained by using a series of band-pass filters (Optical Coatings Japan). The water filter was also

equipped to avoid the heat effects. The AQE at each monochromatic light was calculated by the equation: $AQE = (1 \times \text{the number of acetone molecules}/\text{the number of incident photons}) \times 100\%$. The calculation of quantum efficiency (QE) was conducted according to previous report by using the equation: $QE = (1 \times \text{the number of acetone molecules}/\text{number of photons absorbed})$.

5. Photocatalytic oxygen production from water

0.1 g of catalysts were dispersed by a magnetic stirrer in 270 ml of H₂O in a Pyrex reaction cell. Silver nitrate was added as a sacrificial reagent. A 300W Xe arc lamp (Hayashi Tokei, Luminar Ace 210) equipped with a cutoff filter of 420 nm was employed for the visible-light irradiation. The amount of evolved O₂ was determined using a gas chromatograph (Shimadzu, GC-8A, TCD, Ar carrier).

6. Preparation of photoelectrodes

The photoelectrodes were prepared according to previously reported method.^[3] The indium doped tin oxide (ITO) substrates were cleaned by ultrasonication in distilled water, absolute ethanol, and isopropanol for 15 min sequentially, and then dried in vacuum. 5 mg of photocatalysts and 10 μ l of Nafion solution (5 wt%) were dispersed in 1 ml water/isopropanol mixed solvent (3:1 v/v) by at least 30 min sonication to form a homogeneous catalyst colloid. Then, 150 μ l of the catalyst colloid was deposited onto areas of ca. 1 cm² of the ITO conductive glass and then was dried in air to form the working electrode.

7. Photoelectrochemical measurements in a three-electrode system

The photoelectrochemical properties were investigated in a conventional three-electrode cell by using an electrochemical analyzer (Model-650A). The BiOCl-Au coated ITO glass, a Pt foil, and an Ag/AgCl electrode and 0.5 M Na₂SO₄ aqueous solution were used as the working electrode, the counter-electrode, the reference electrode and the electrolyte, respectively. A 500 W Xe arc lamp equipped with a 420 nm cutoff filter was utilized as a light source. Electrochemical impedance spectra (EIS) were recorded at an applied potential of 0.23 V vs. Ag/AgCl over the frequency range of 1 MHz to 0.01 Hz. The photocurrent with ON/OFF cycles was measured at an applied potential of 0.5 V vs. Ag/AgCl. Mott-Schottky plots were obtained under direct current potential polarization at a frequency of 1 kHz. The potential ranged from -0.8 to 1.4 V (vs. Ag/AgCl).

8. Photoelectrochemical measurements in a two-electrode system

Photoelectrochemical measurements in the two-electrode system were carried out according to Tada's report.^[4] Both the working electrode and the counter-electrode are composed of BiOCl-Au electrodes. 0.1 M Na₂SO₄ aqueous solution containing 5 wt% 2-propanol was used as electrolyte. Under visible-light illumination by a 500 W Xe arc lamp equipped with a 420 nm cutoff filter, the photocurrent was evaluated without external bias.

9. Theoretical calculation

The DOS plots of BiOCl-001 and BiOCl-010 were obtained by using the first principles DFT calculations to specify the electronic structure of {001} and {010} facets in this photocatalyst. In this work, all calculations were performed with the Vienna ab-initio Simulation Package (VASP).^[5] The Projector-augmented wave (PAW) was used for the electron-ion interactions. The generalized gradient approximation (GGA) with PBE functional was employed to evaluate the exchange-correlation energy.

During the geometrical optimization, the energy and force converged to 5×10^{-6} eV/atom and 0.01 eV/Å, respectively. The k-points meshes for BiOCl-bulk, BiOCl-001 and BiOCl-010 were $6 \times 6 \times 3$, $7 \times 7 \times 1$ and $7 \times 4 \times 1$, respectively. For slab calculations, the vacuum layer was set to 18 Å which can ignore the interaction between neighboring structural models. And the slab models for BiOCl-001 and BiOCl-010 include 11 and 7 atomic layers, respectively. Additionally, the equations of surface energy calculations were similar with the method presented in Ref. [9].

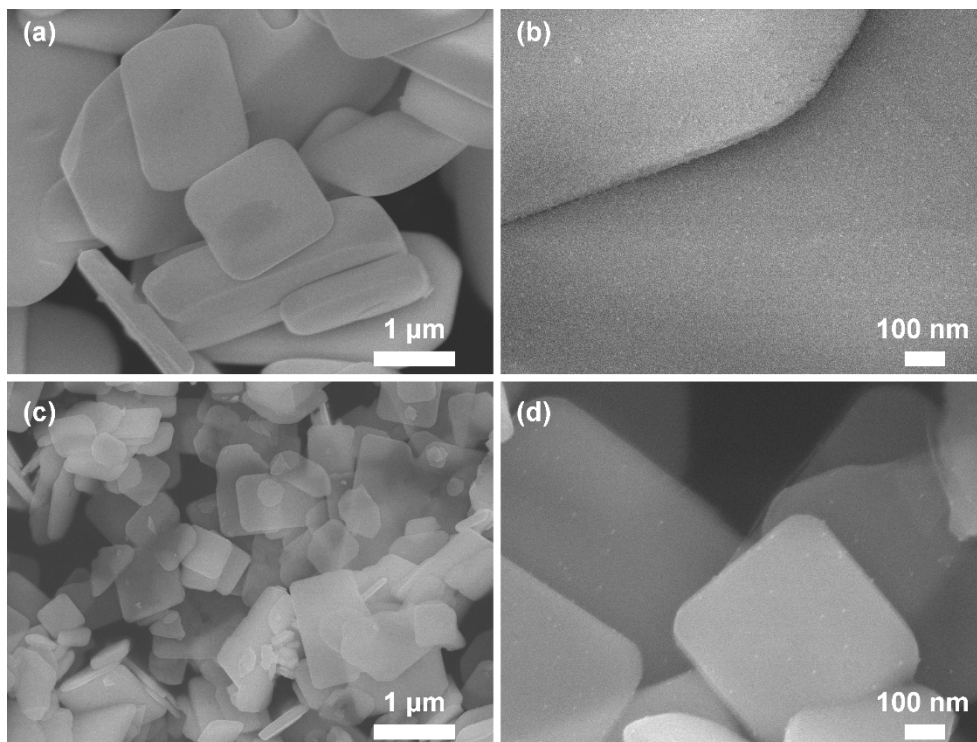


Figure S1. SEM images of (a, b) BiOCl-001-Au and (c, d) BiOCl-010-Au. The images (b, and d) show that Au nanoparticles are well-dispersed on the {001} and {010} facets of BiOCl nanosheets for BiOCl-001-Au and BiOCl-010-Au samples, respectively.

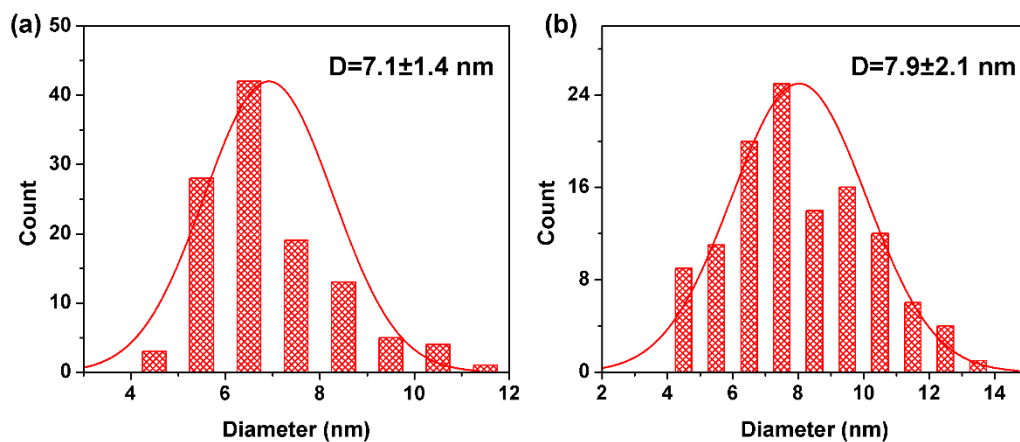


Figure S2. Diameter histograms of Au nanoparticles (a) BiOCl-001-Au and (b) BiOCl-010-Au and they are plotted based on ≥ 100 particles.

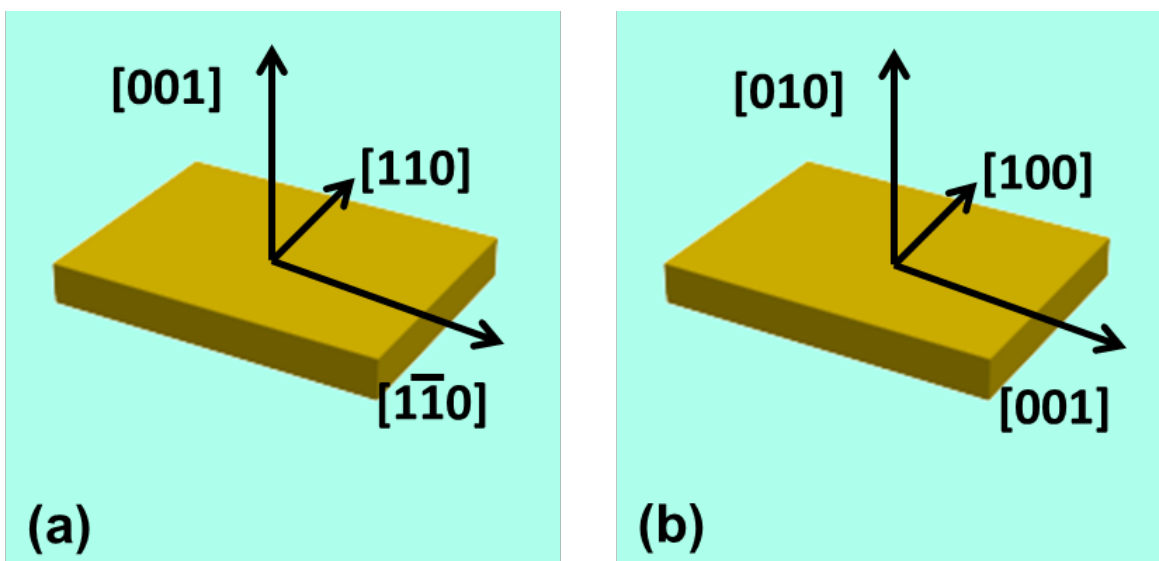


Figure S3. Schematic illustration of the crystal orientation for (a) BiOCl-001 and (b) BiOCl-010.

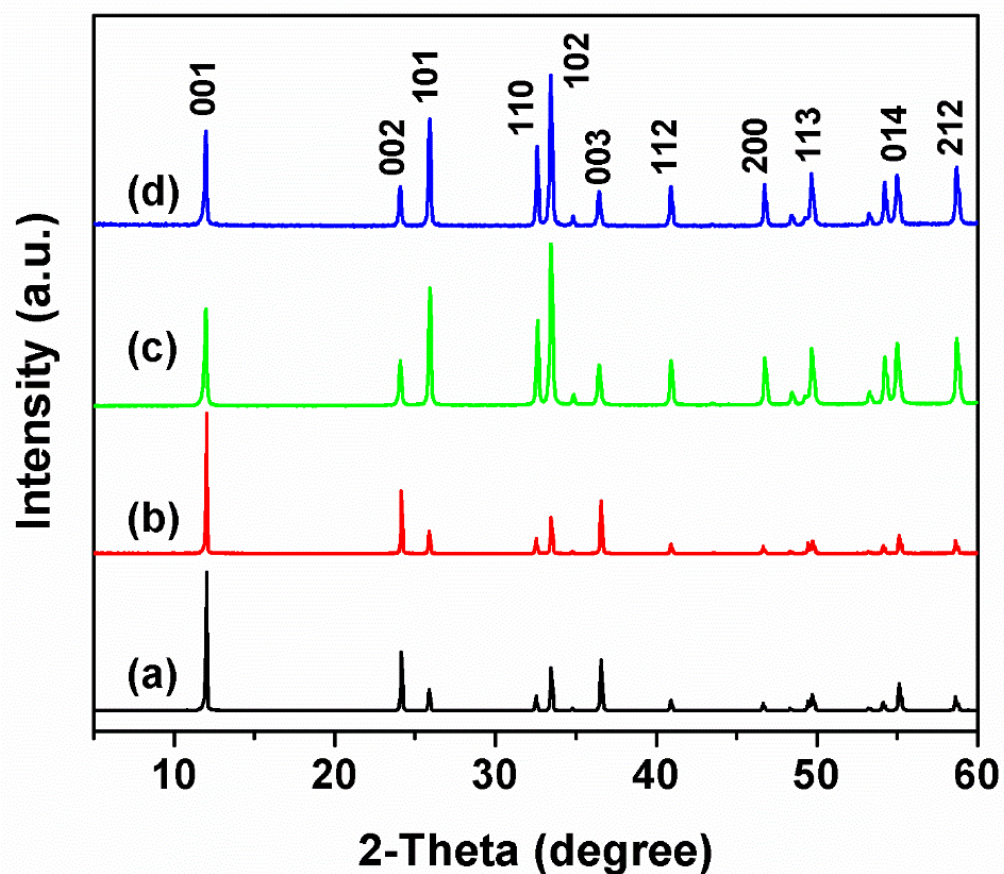


Figure S4. XRD patterns of (a) BiOCl-001, (b) BiOCl-001-Au, (c) BiOCl-010, and (d) BiOCl-010-Au. No peaks belong to Au were detected in BiOCl-001-Au and BiOCl-010-Au. It may be because the loading amounts of Au is below the XRD detection limit.

Table S1. The intensity ratios of the (002) and (200) peaks in various samples.^a

Sample	$R=I_{002}/I_{200}$
BiOCl-001	6.88
BiOCl-001-Au	7.12
BiOCl-010	0.81
BiOCl-010-Au	0.79

^a From the XRD patterns, the intensity ratios of the (002) and (200) peaks were calculated to be 6.88 and 0.81 for BiOCl-001 and BiOCl-010, respectively, nearly equal to the values reported by Zhang et al.^[1] These results provide additional evidences for the selective formation of BiOCl nanosheets with exposed {001} and {010} facets.

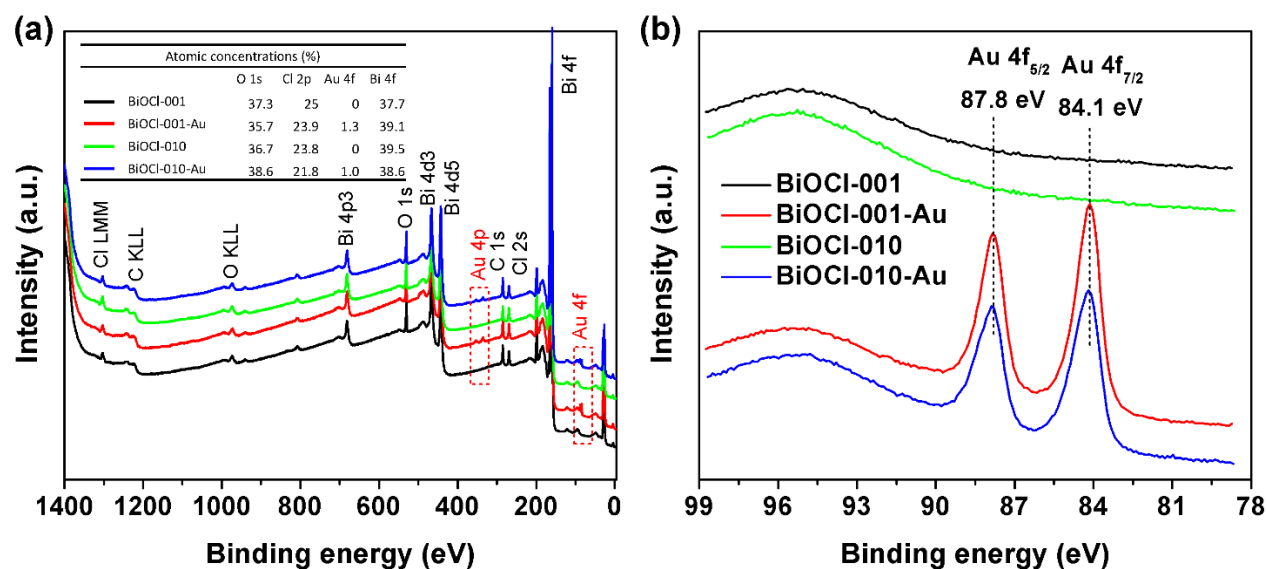


Figure S5. XPS spectra of BiOCl-001, BiOCl-001-Au, BiOCl-010, and BiOCl-010-Au: (a) survey and (b) Au 4f. The loading amounts of Au in BiOCl-001-Au and BiOCl-010-Au are determined to be 0.9 and 0.7 at.%, respectively.

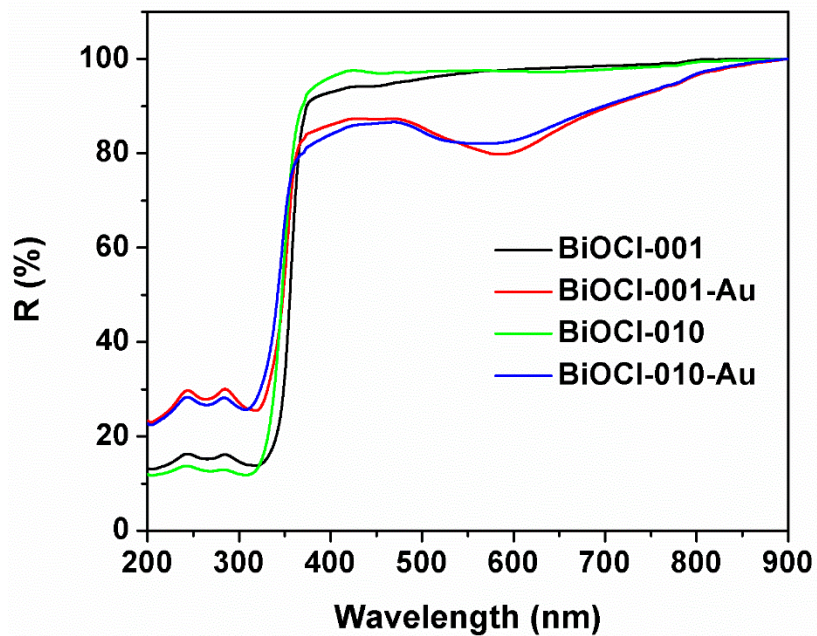


Figure S6. UV-vis diffuse reflectance spectra of BiOCl-001, BiOCl-001-Au, BiOCl-010, and BiOCl-010-Au.

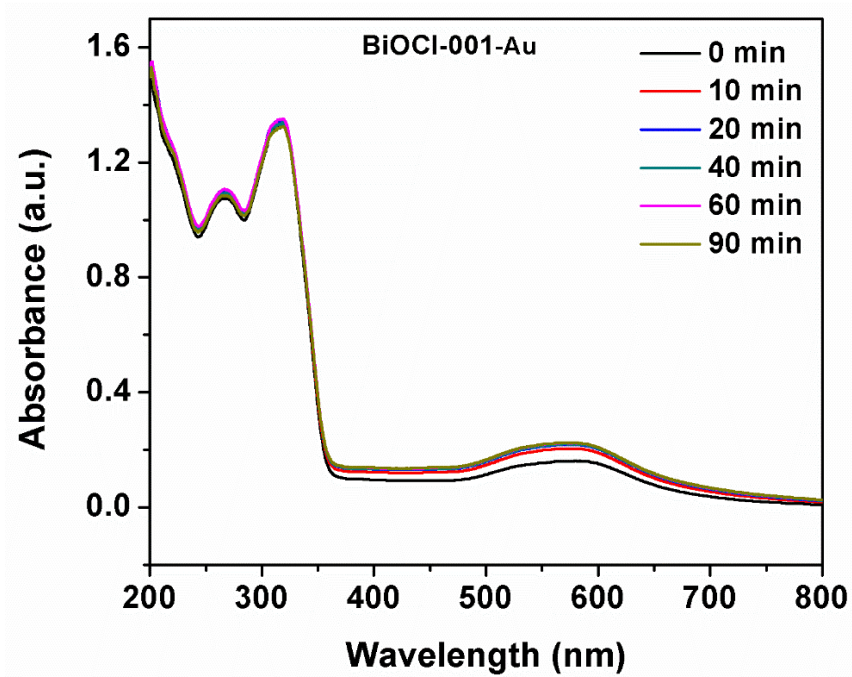


Figure S7. UV-vis absorption spectra of BiOCl-001-Au in Ar-saturated methanol during visible-light irradiation.

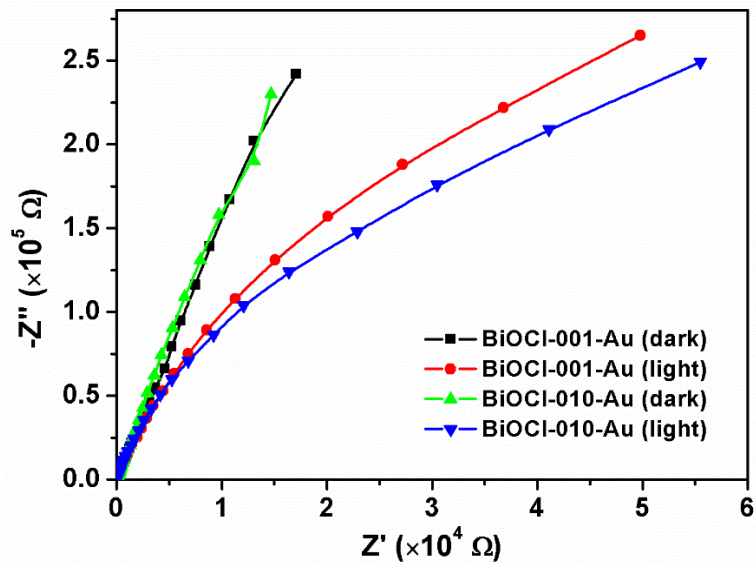


Figure S8. Nyquist plots of electrochemical impedance spectra of BiOCl-001-Au and BiOCl-010-Au in the dark and visible-light.

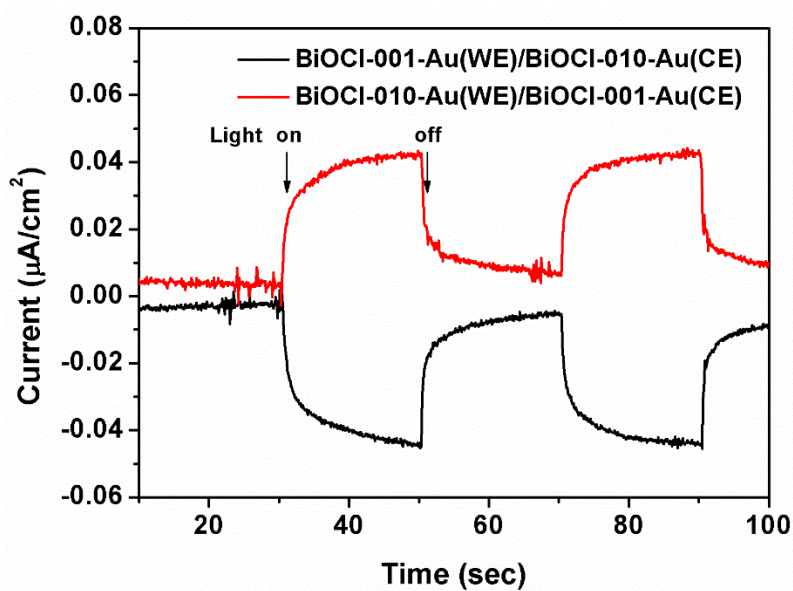
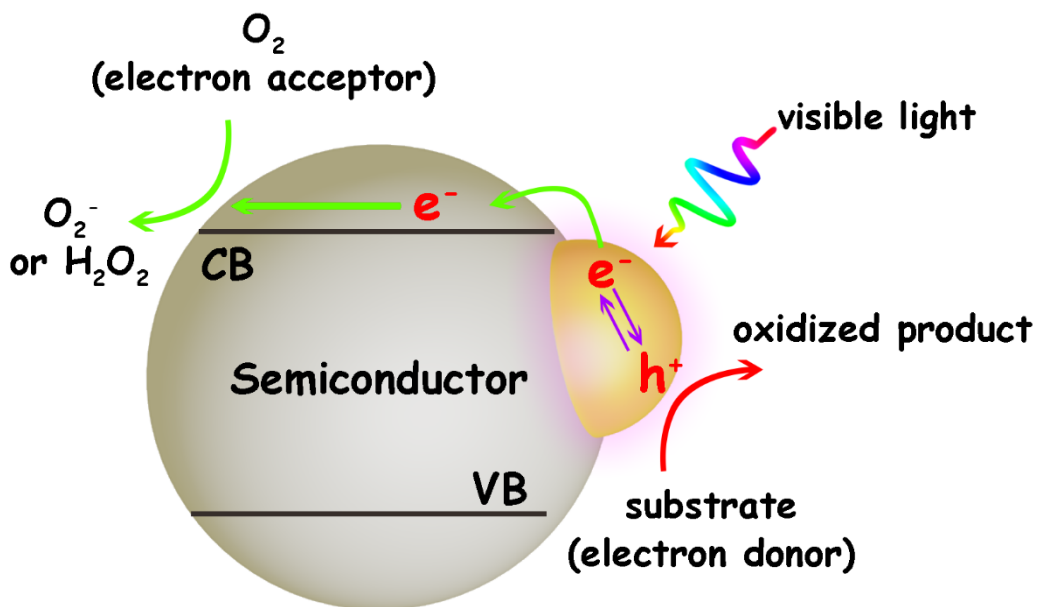


Figure S9. Photocurrent responses for the two electrode system employing BiOCl-001-Au and BiOCl-010-Au as working electrode and counter electrode under visible-light illumination (without external bias).



Scheme S1. Proposed mechanism for aerobic oxidation through the SPR of Au particles supported on semiconductor particles under visible-light irradiation.

As shown in Scheme 1, aerobic oxidation through the SPR of Au particles involves two stages:^[6] Firstly, visible-light induced collective oscillation of electrons on the Au particles injects hot electrons into the conduction band of semiconductor supports, leaving the holes in the Au particles. Secondly, injected hot electrons in semiconductor supports contribute to reduction of O_2 (electron acceptor) and simultaneously holes in Au particles participate in the oxidation of organic substrate (electron donor, *e.g.* isopropanol). Based on this, oxidation of organic substrate has been considered to be a good index to indicate the hot electron transfer in plasmonic photocatalysts.^[6-7] According to our previous report,^[7a, 7c, 8] different from the aerobic oxidation which can be driven by SPR excitation of Au particles, water oxidation over plasmonic photocatalysts usually involves an Au interband transition process because a relative higher energy is needed for holes to oxidize water to form O_2 . However, both processes can be the reflection of hot electron transfer.^[7a, 7c, 8]

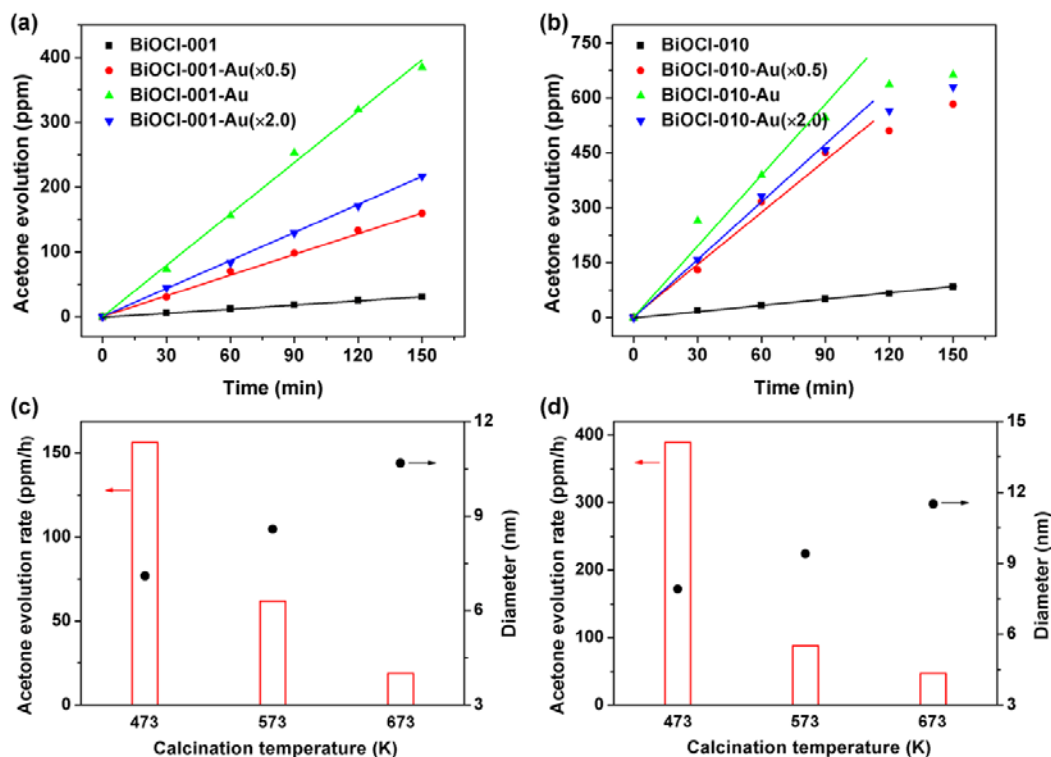


Figure S10. (a, b) Acetone evolutions over (a) BiOCI-001-Au and (b) BiOCI-010-Au with different Au loading amounts. The “BiOCI-001-Au(×0.5)” and “BiOCI-010-Au(×0.5)” indicate that the Au loading amount is half of the normal case (Normal case: 0.9 and 0.7 at.% for BiOCI-001-Au and BiOCI-010-Au, respectively). The “BiOCI-001-Au(×2)” and “BiOCI-010-Au(×2)” indicate that the Au loading amount is double of the normal case. (c, d) Acetone evolution rates of (c) BiOCI-001-Au and (d) BiOCI-010-Au with various Au nanoparticle diameters. The diameters of Au nanoparticles were controlled by annealing the samples at different temperatures. From c and d, with the Au particle diameter increasing, the activities for both BiOCI-001-Au and BiOCI-010-Au were shown to be dramatically decreased.

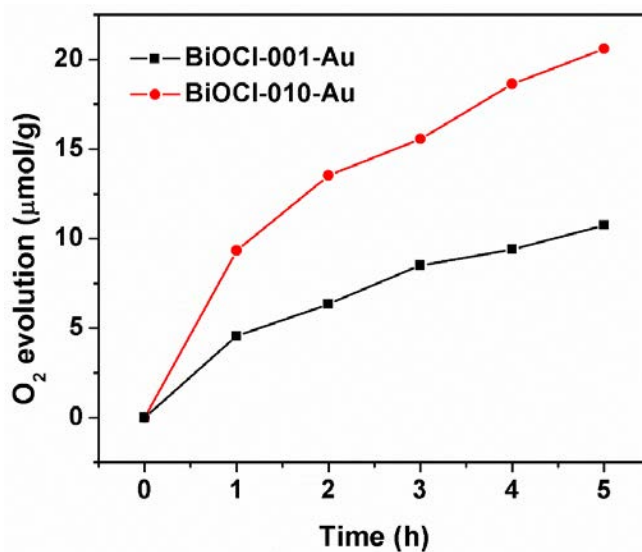


Figure S11. Oxygen productions from water over (a) BiOCI-001-Au and (b) BiOCI-010-Au.

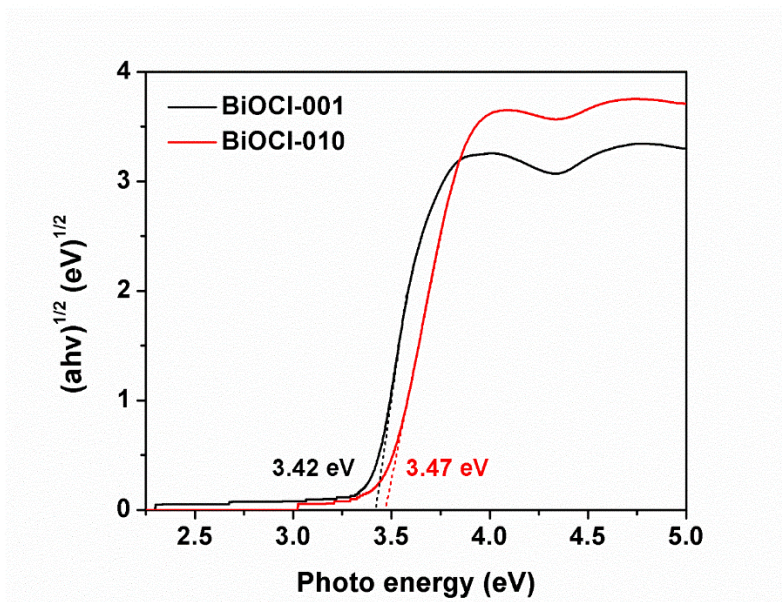


Figure S12. $(ah\nu)^{1/2}$ versus $h\nu$ plots of BiOCl-001 and BiOCl-010, showing that the corresponding band gaps are 3.42 and 3.47 eV, respectively.

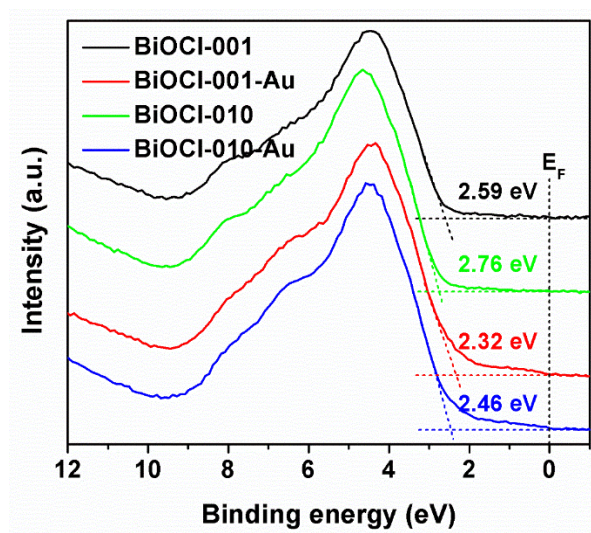


Figure S13. The valence band XPS spectra of BiOCl-001, BiOCl-001-Au, BiOCl-010, and BiOCl-010-Au. Obviously, the valence bands of BiOCl-001 and BiOCl-010 lie at 2.59 and 2.76 eV below the corresponding Fermi levels, respectively.

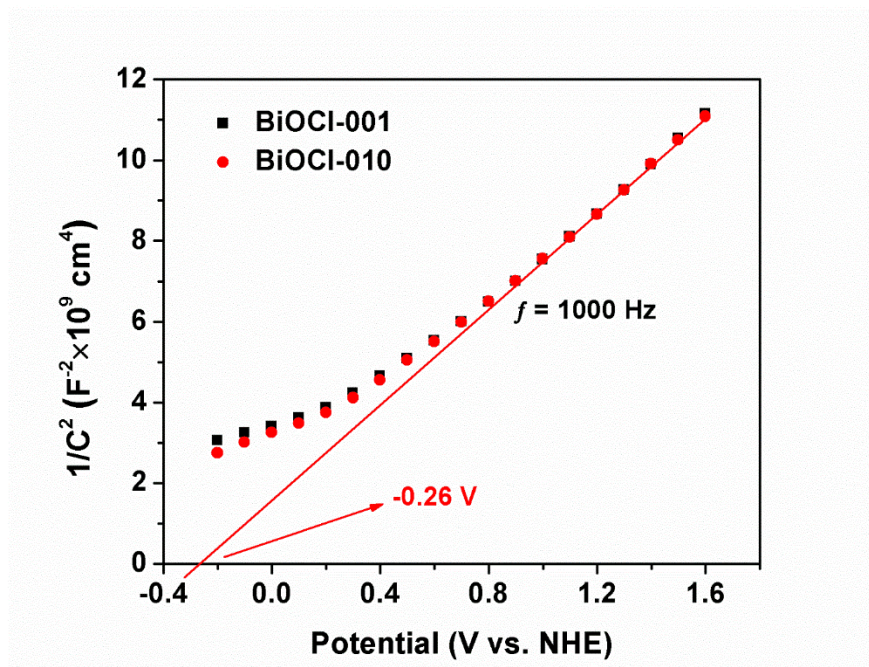


Figure S14. Mott-Schottky plots of BiOCl-001 and BiOCl-010. It shows that both BiOCl-001 and BiOCl-010 are n-type semiconductors and that they present the same Fermi level of -0.26 V (vs. NHE).

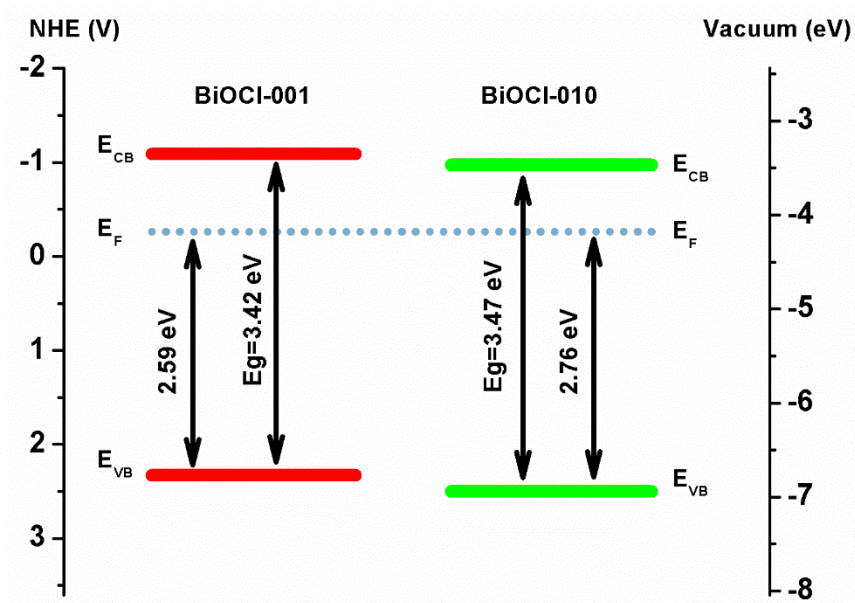


Figure S15. Schematic band structures of BiOCl-001 and BiOCl-010.

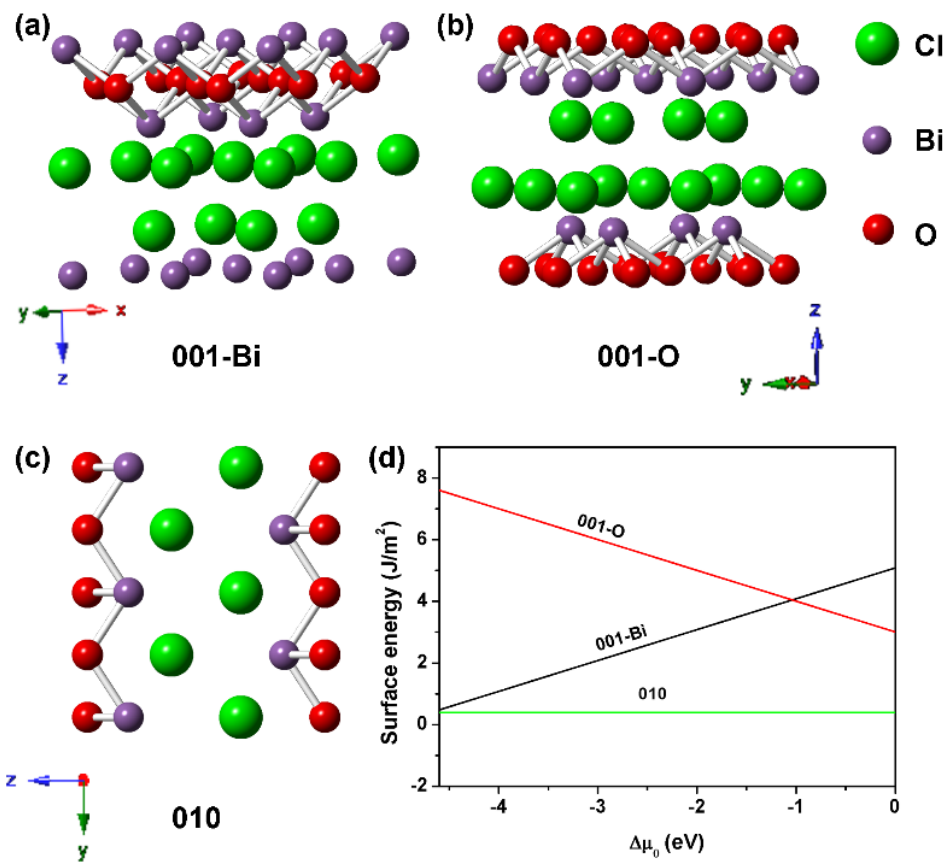


Figure S16. (a-c) Schematic of atomic surface structure of BiOCl: (a) (001-Bi), (b) (001-O), and (c) (010). (d) Calculated surface energies for (001-Bi), (001-O), and (010). The surface energy of (001) surface with Cl termination was not taken into account because the Cl atoms are connected by the nonbonding van der Waals. In (d), the surface energy of (001-Bi) surface increases with the upshift of the chemical potential of oxygen (μ_0). This is indicative of the instability of (001-Bi) surface in O-rich environments. In contrast, (001-O) surface is relatively stable in O-rich environments. The surface energies of (001-O) and (010) are estimated to be 3.00 and 0.39 J/m², respectively. These results are consistent with previous report.^[9]

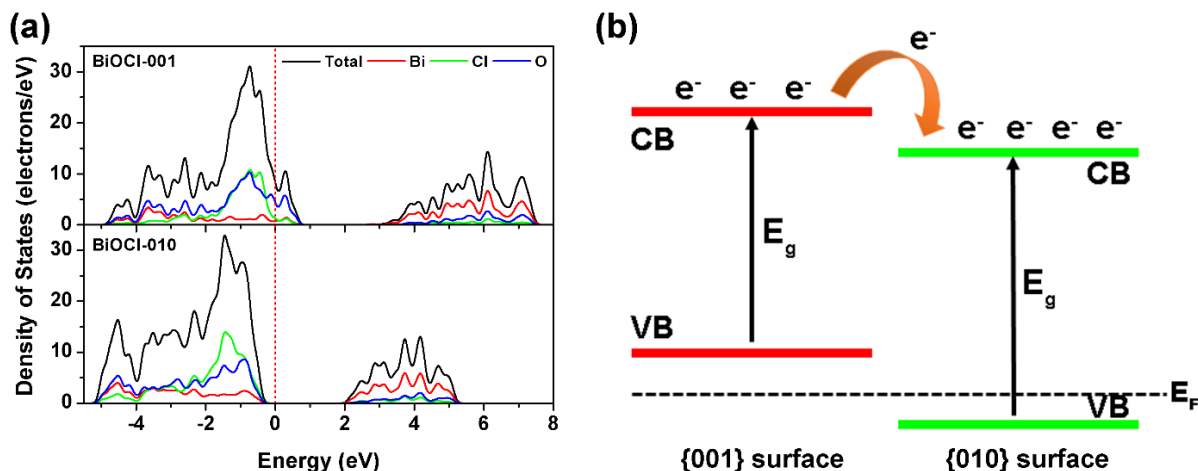


Figure S17. (a) Density of states (DOS) plots for {001} and {010} surface of BiOCl. (b) Schematic of surface heterojunction between {001} and {010} in BiOCl. Based on the surface energy calculation, O terminated (001) surface is much more stable than that terminated by Bi. Accordingly, the DOS calculation was performed for (001-O) surface. As shown in (a), the Fermi level of {001} facets in BiOCl enters their valence band because of the dangling bonds presented at surface oxygen atoms. By contrast, the Fermi level is still located at the top of the valence band for {101} facets. When {001} and {010} facets are contacted, their Fermi levels should be equal. If there are some free electrons on the conduction band of {001} facets (e.g. the electrons coming from SPR induced hot electron injection), the electrons would prefer to migrate into the conduction band of {010} facets due to its relatively lower potential level. These results suggest that the {010} facets in BiOCl significantly favor accumulating electrons over the {001} facets. Similar results were also reported by other researchers.^[10]

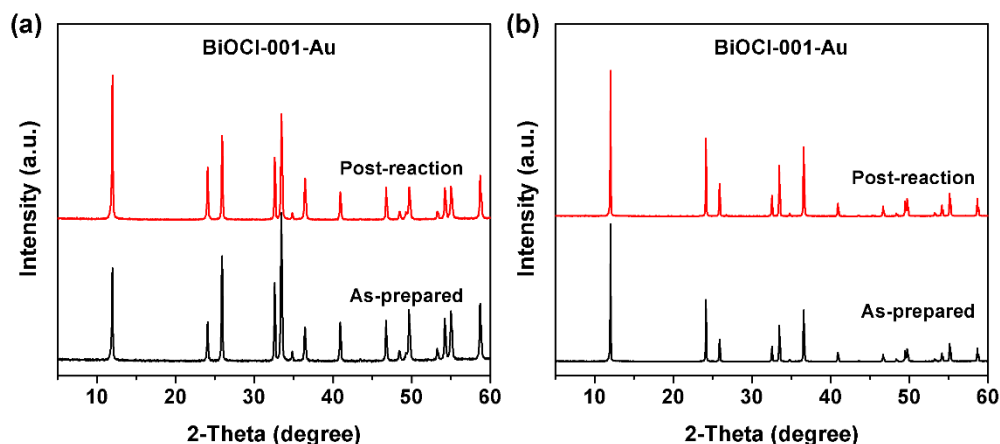


Figure S18. Comparison of XRD patterns for (a) BiOCl-001-Au and (b) BiOCl-010-Au before and after the photooxidation of IPA. Obviously, no obvious difference appears during the reaction for both two catalysts, indicating their good stabilities.

References

- [1] J. Jiang, K. Zhao, X. Xiao, L. Zhang, *J. Am. Chem. Soc.* **2012**, *134*, 4473.
- [2] C. Gomes Silva, R. Juárez, T. Marino, R. Molinari, H. García, *J. Am. Chem. Soc.* **2010**, *133*, 595.
- [3] X. Yu, A. Shavel, X. An, Z. Luo, M. Ibáñez, A. Cabot, *J. Am. Chem. Soc.* **2014**, *136*, 9236.

- [4] S.-i. Naya, T. Niwa, T. Kume, H. Tada, *Angew. Chem. Int. Ed.* **2014**, *53*, 7305.
- [5] J. Kim, D. Monllor-Satoca, W. Choi, *Energy Environ. Sci.* **2012**, *5*, 7647.
- [6] D. Tsukamoto, Y. Shiraishi, Y. Sugano, S. Ichikawa, S. Tanaka, T. Hirai, *J. Am. Chem. Soc.* **2012**, *134*, 6309.
- [7] (a) L. Liu, T. D. Dao, R. Kodiyath, Q. Kang, H. Abe, T. Nagao, J. Ye, *Adv. Funct. Mater.* **2014**, *24*, 7754; (b) Z. Bian, T. Tachikawa, P. Zhang, M. Fujitsuka, T. Majima, *J. Am. Chem. Soc.* **2013**, *136*, 458; (c) L. Liu, S. Ouyang, J. Ye, *Angew Chem Int Ed* **2013**, *52*, 6689.
- [8] L. Liu, P. Li, B. Adisak, S. Ouyang, N. Umezawa, J. Ye, R. Kodiyath, T. Tanabe, G. V. Ramesh, S. Ueda, H. Abe, *J. Mater. Chem. A* **2014**, *2*, 9875.
- [9] K. Zhao, L. Zhang, J. Wang, Q. Li, W. He, J. J. Yin, *J. Am. Chem. Soc.* **2013**, *135*, 15750.
- [10] J. Yu, J. Low, W. Xiao, P. Zhou, M. Jaroniec, *J. Am. Chem. Soc.* **2014**, *136*, 8839.